Nuclear Materials and Energy 17 (2018) 9–14

Contents lists available at ScienceDirect

Nuclear Materials and Energy

journal homepage: www.elsevier.com/locate/nme

HiperFer, a reduced activation ferritic steel tested for nuclear fusion applications

S. Möller*, B. Kuhn, R. Rayaprolu, S. Heuer, M. Rasinski, A. Kreter

Forschungszentrum Jülich GmbH, Institute of Energy and Climate Research (IEK), Jülich 52425, Germany

ARTICLE INFO

Keywords:
Nuclear material
Steel
Activation
Plasma-facing material
Structural material
Nuclear fusion

ABSTRACT

Materials are the most urgent issue in nuclear fusion research. Besides tungsten, steels are considered for unifying functional and structural materials due to their cost and mechanical advantages over tungsten. However, the fusion neutrons impose a strong constraint on the ingredients of the steel in order to avoid long lasting activation, while the material has to pertain sputtering resistance, low hydrogen retention, and long-term mechanical stability. In this proof-of-principle, we demonstrate the interesting properties of the new material HiperFer (High performance Ferrite) as a material suitable for fusion applications.

The investigation covers neutron activation modelled by FISPACT-II, plasma sputtering and deuterium retention experiments in PSI-2, thermo-mechanical properties and component modelling. The material was found to feature a low nuclear inventory. Its sputtering yield reduces due to preferential sputtering by a factor 4 over the PSI-2 D_2 plasma exposure with possible reductions of up to 70 indicated by SD.Trim.SP5 modelling. The exposure temperature shows a strong influence on this reduction due to metal diffusion, affecting layers of 1 μm in PSI-2 at 1150 K exposure for 4 h. Deuterium retention in the ppm range was found under all conditions, together with ~10 ppm C and N solubility of the ferritic material. The creep and cyclic fatigue resistance exceed the values of Eu-97 steel. As an all HiperFer component, heat loads in the order of 1.5 MW/m^2 could be tolerated using water-cooled monoblocks. In conclusion, the material solves several contradictions present with alternative reduced-activation steels, but its applications temperatures >820 K also introduce new engineering challenges.

1. Introduction

Plasma-facing-materials were, so far, selected according to plasma physics requirements, leading to special materials with high purity such as Be or W. In future reactors engineering issues will become more important than plasma physics, introducing a paradigm shift in material selection. Therefore, materials with excellent engineering (strength, ductility, fatigue life) and processing properties (welding, casting) will be required, but still keeping their plasma properties, nuclear activation, and product cost in mind.

Steels naturally provide a good compromise in this space of qualities. Several types were already developed for nuclear fusion applications with Eu-97 [1] being one of the most prominent types. Since the development of Eu-97 steel research in fusion and other fields revealed several weaknesses and relevant improvements, leading to e.g. the so-called generation 3 and 4 ferritic-martensitic steels [2]. The HiperFer steel [3] originally intended for highly efficient and dynamic conventional power plants is in line with several ideas of these new developments and beyond. HiperFer is a ferritic steel requiring five functional ingredients (Fe, Cr, Si, W, and Nb or Ta) which are acceptable from a nuclear activation point of view. The material is strengthened by intermetallic Laves phases (typically AB_2), giving the material good high-temperature creep strength and mechanical fatigue strength. At the same time, the high W content for the Laves phases in the order of 3–6 wt% offers the prospect of good plasma sputtering resistance. The high Cr content suffices to allow for hot-steam oxidation resistance as passive safety mechanism in a loss of coolant event.

This study aims at evaluating HiperFer for use in a nuclear fusion environment. Samples from two casts of the material with 18–21 at.% Cr, 0.8–1.2 at.% W, 0.5% Si, and 0.5 at.% Nb were available for testing. The study includes plasma exposures in PSI-2 [4], thermo-mechanical data, compositional analysis, hydrogen retention, thermal and nuclear modelling. The comparison with W and other steels allows judging the relative performance of HiperFer. Finally perspectives for further optimization of the material towards nuclear fusion applications and future experiments will be given.

* Corresponding author.
E-mail address: s.moeller@fz-juelich.de (S. Möller).

https://doi.org/10.1016/j.nme.2018.06.010
Received 8 February 2018; Received in revised form 6 June 2018; Accepted 10 June 2018

Table 1
Composition of HiperFer W4 analysed by ICP-OES and LECO CS/TCH 600 with uncertainties <10%.

Weight %	Fe	Cr	Nb	Si	Mn	Co	Ni	W	C	S	N	O
HiperFerW4	75.1	16.5	1.0	0.3	0.186	0.0067	0.0081	4.2	0.002	0.001	0.004	0.005

2. Material aspects

The HiperFer steel was produced specifically for testing by casting in batches of 80 kg. CroFer®22H and W reference materials were commercially produced. The used W material produced by Plansee has a purity of 99.994% and corresponds to ITER specifications. It is identical to W materials used in all fusion experiments at Forschungszentrum Jülich. HiperFer was not specifically heat-treated (i.e. it entered the relevant tests without strengthening Laves phase particles), prior to the experiments, neither were the other materials thermally modified. All samples were polished on the plasma-exposed surfaces using diamond suspensions to a roughness of $R_a \approx 12$ nm.

The HiperFer with 4 wt% W (HiperFerW4) was analysed by inductively coupled plasma with optical emission spectroscopy for its metallic composition down to the 10 ppm detection limit of the applied device. The composition is depicted in Table 1. C, N, O, S were analysed by LECO CS/TCH 600 analysers (infrared absorption of outgassing). The magnetic properties of the steel were not quantitatively characterized, but a clear ferromagnetic behaviour, similar to Eu-97, was present. Tests revealed a good adhesion of HiperFer-HiperFer diffusion welding bonds starting from 920 K. Also connections with W, e.g. as additional armour are possible and under investigation. As the material can be cast and welded, complex geometries and manufacturing are in general unproblematic and low overall cost can be expected for a reactor construction.

HiperFer features several specific strength for applications above 820 K. At temperatures above 950 K, the mechanical parameters significantly deteriorate, but a non-structural operation remains possible at least up to 1150 K, as demonstrated below. At temperatures in the range of 600–820 K, reversible structural changes slowly embrittle the steel, requiring at least regular heating above 840 K for recovery. HiperFer's Cr content leads to two orders of magnitude lower high-temperature steam oxidation rates compared to 9% ferritic-martensitic steels (see “18Cr” alloy vs. P92 in [3]) such as Eu-97, making it suitable for supercritical-steam based power plants. The application of HiperFer therefore suggests coolant temperatures of 820–950 K, leading to about twice the thermal to electric conversion efficiency compared to ~550 K coolant temperature concepts for fusion reactors. Especially in nuclear environments, where Nickel based alloys are not applicable, HiperFer might be the only available structural reduced-activation material applicable for this exceptional conversion efficiency. Additionally, not being dependent on carbides makes it potentially more stable in hydrogen environments such as nuclear fusion. On the other hand, >820 K introduces new engineering challenges for a reactor design and the use of liquid metals might be difficult at these high temperatures. Tolerable power load densities on plasma-facing components could also be lower due to the limited temperature difference of about 300 K. In contrast to fission reactors, where the water coolant temperatures are limited to the sub-critical range due to the direct contact to the fuel elements, fusion reactors offer a high degree of flexibility in selecting (supercritical) coolant temperatures, allowing for this improved economics and radiation resistance.

The engineering properties such as tensile properties, fatigue lifetime, and creep are discussed in separate papers [5,3]. In general, HiperFer has exceptional engineering parameters and lifetime under cyclic loads at high temperatures. In comparison to non-Laves phase steels the values are significantly improved. For example, the creep rupture strength improves by a factor of up to two (Fig. 1). Furthermore, the thermal expansion is about 10% smaller compared to T92, which is similar to Eu-97, as depicted in Fig. 2.

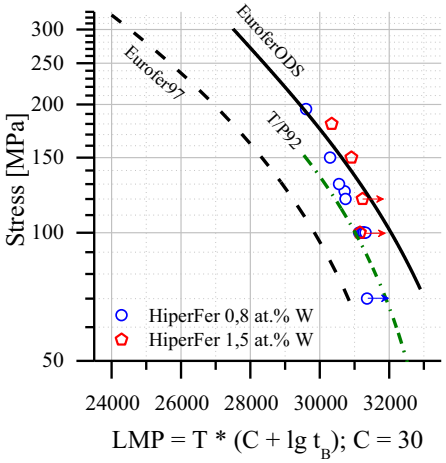

Fig. 1. Creep rupture strength analysis with comparison to other steels. The data were generalised by the Larson–Miller relation with a constant of C = 30 to the Larson-Miller parameter (LMP). Arrows indicate ongoing experiments. Eurofer97 data were taken from [1], EuroferODS from [6], and T/P92 data from [7].

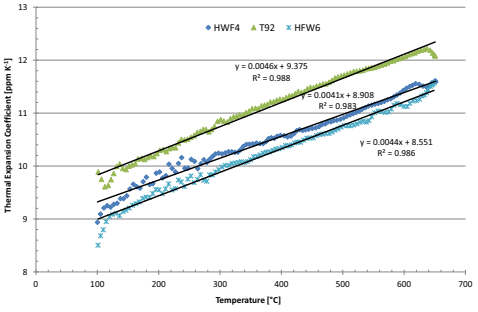

Fig. 2. Thermal expansion measured for both HiperFer variants and T92 (similar to Eu-97) from 370 K to 925 K. Linear fits and resulting parameters next to each dataset. The expansion clearly reduces with higher W content of the steel.

3. Nuclear properties

Low neutron activation is a decisive factor for qualification of fusion reactor materials. Use of MCNP6 [8] calculated neutron flux as input into FISPACT-II [9], an inventory calculation program, is the present norm for activation prediction of reactor materials. Fluxes corresponding to a 1.6 GW fusion power DEMO reactor were obtained from work performed in [10] and inserted as a 709 energy group into FISPACT-II. Using TENDL-2015 [11], computations were performed for the activation of HiperFer with Nb and Ta alloying, Eu-97, pure W, and pure Fe similar to the calculations presented in [12]. A 30% availability of DEMO was considered using proportionally reduced average neutron flux over 2 years, in line to the start-up blanket forecast [13] for reasons of comparability to literature. For the steels, measured impurity concentrations were considered in the calculations. HiperFer-Nb and HiperFer-Ta were assumed to feature the same composition, except for a 1:1 atomic substitution of Nb for Ta. The results shown in Fig. 3 exhibit relevant differences between the steels and Fe only after 10 years of cooling. After 10 years, Fe features the lowest activity, closely followed by HiperFer-Ta. Eu-97 remains on a 10 times and HipferFer-Nb on a

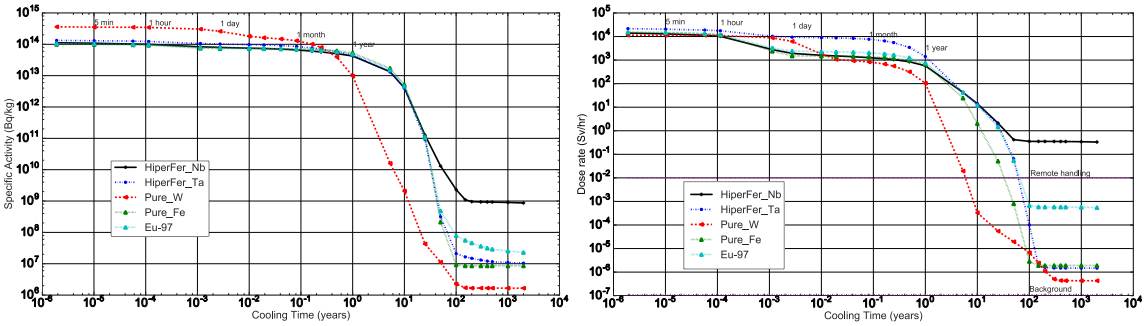

Fig. 3. Specific activity and dose rate of different materials considered for fusion applications after DEMO start-up irradiation. HiperFer-Ta and W offer the best prospects to re-use the material after some hundred years. Besides handling cost aspects, a fast activity decay is also relevant for accident scenarios and social acceptance.

100 times higher activity level. Advantages of HiperFer-Ta against Eu-97 arise from the 10 times lower C and N solubility, leading to lower levels of long-lived ^{14}C and ^{10}Be, and the high purity of the investigated HiperFer batch regarding Ni and Co (similar to Eu-97). The main contribution to the activity of HiperFer-Ta originates from the Mn-53 isotope mostly produced from the Fe part of the alloy.

In order to give an estimate for the clearance times of the materials, we compare the results to German legislation (Strahlenschutzverordnung – StrlSchV 20.7.2001 (BGBl. I S. 1714; 2002 I S. 1459)). The legislation allows for an activity of Mn-53 of 10^7 Bq/kg for releasing the material to non-radioactive scrap-metal recycling. According to the modelling, this level could be reached after about 1000 years with an uncertainty of −900 and $+10^7$ years of cooling time. The large error bar derives from the TENDL cross-sections and neutron spectrum used for the calculation, each having a factor 3 systematic uncertainty, and the long half-life of Mn-53 (3.74 Myear half-life). Among this, several impurity contents (especially Ni and Co) solely depend on the production quality and therefore will be different for different final products, although the differences introduced by production upscaling are expected to be small. Interestingly, HiperFer-Ta and Fe, could be released under German legislation significantly earlier from fusion reactors than W and Eu-97 due to the 10 times higher release limits of Mn-53 compared to the main isotope in W (Re-186) and the 10 times lower residual C in a ferrite (HiperFer) compared to a martensite (Eu-97) leading to less C-14 production. In fission reactors, in contrast, the stronger thermal neutron component would mostly lead to Co-60 production from Fe, which remains problematic for orders of magnitude longer than Mn-53. In spite of this, even with fission neutrons the long-term activity of HiperFer remains orders of magnitude lower compared to Ni containing steels which are considered as alternative for operation >820 K. In conclusion, HiperFer-Ta potentially represents a suitable material for a D-T fusion reactor considering its activation properties, but the final material production and irradiation conditions will be very decisive for its activation properties.

The irradiation damage during reactor exposure constitutes the second large block of relevant nuclear properties of a fusion material. Experiments are complicated and therefore only qualitative comparisons between different materials can be given at this point. In general, steels will suffer from about 2 to 3 orders of magnitude more gas and 2 times more displacements than tungsten under the same neutron load. This potential drawback is contrasted by faster diffusion, annealing, and better mechanical properties. In particular, HiperFer differs from Eu-97 in requiring and tolerating higher application temperatures due to its different structure. The hardening by Laves particles and the purely ferritic/α phase allow stable operation at temperatures >820 K with accelerated annealing and outgassing of damage. The high temperatures furthermore enable α-α' phase stability for steam-passivating Cr-content <20 at. % (see [14] Fig. 1) leading to additional passive safety in loss-of-coolant-accidents. Experimental screening of steels by neutron and ion beams [15] is required for robust statements on irradiation lifetime.

4. Plasma-material interaction

The resistance to heat and particle loads and sputtering by plasma particles represents critical challenges for a material intended as a functional or, respectively, plasma-facing material in a nuclear fusion reactor. Experimental tests of HiperFer were conducted in the linear plasma experiment PSI-2 [4]. Here several samples were exposed to a D_2 plasma with a peak flux of $6 \pm 1 \times 10^{21}$ D^+/m^2s for 4 h at floating potential of 50 V. Eight mirror-finished samples of $10 \times 10 \times 5$ mm^3 were exposed in each experiment. The set consisted of two HiperFer W6 (1.2 at. % W), HiperFer W4 (0.8 at% W), Crofer 22H (0.55 at. % W), and 99.994% W with both samples of the same type mounted 180° apart. The sample surface temperatures were continuously monitored with an accuracy of ± 2% via referenced infrared imaging as described in [16].

After the exposures, all samples were analysed post-mortem by electron microscopy, weight-loss, and ion-beam analysis. The weight of each sample was measured before and directly after exposure using a Mettler Toledo XP6U with an accuracy of ± 2 μg. Only the W samples were weighted with a Sartorius Cubis with ± 10 μm due to their higher density/weight. Results of the pre-post comparison of the mass-loss are depicted in Table 2. About 2 month after the exposure, the samples

Table 2
Exposure conditions and results of mass-loss and ion-beam analysis. HF = HiperFer. The sputtering yield was calculated using the mass-loss, the average atomic weight and a fixed fluence of 8.6×10^{25} D/m^2. W_{Max} specifies the maximum W concentration in the first RBS resolution bin, while D_{Ret} states the D concentration in a depth of 2–5 μm. The table arrangement follows the exposure arrangement.

Sample	T [K]	mass-loss [μg]	Sputter yield	W_{max} [%]	D_{ret} [parts]
HFW6	526	626	7.87E−04	7.50	<2E−07
HFW4	521	658	8.27E−04	7	<1E−07
Crofer	507	642	8.07E−04	6.5	1.0E-06
W	498	73	2.78E−05	100	1.1E−03
HFW6	611	905	1.14E−03	13	3.5E−07
HFW4	549	714	8.98E−04	9	5.0E−07
Crofer	537	475	5.97E−04	6.5	8.0E−07
W	505	65	2.47E−05	100	2.8E−04
HFW6	1069	2729	3.43E−03	5.8	6.0E−07
HFW4	1075	3008	3.78E−03	4.2	<6E−07
Crofer	1085	2436	3.06E−03	2.8	5.0E−06
W	1068	47	1.79E−05	100	<5E−07
HFW6	1149	3523	4.43E−03	8	5.0E−06
HFW4	1158	3458	4.35E−03	5	<3E−07
Crofer	1138	2475	3.11E−03	2.8	6.0E−06
W	1037	93	3.54E−05	100	<5E−07

were analysed by 2.95–4.5 MeV ^{3}He ion-beam analysis with nuclear reaction analysis (NRA) and Rutherford backscattering spectrometry (RBS). The data were evaluated using SimNRA 7.0 [17] and Multi-simnra [18]. The enrichment of W on the sample surface was quantified with an uncertainty of ± 10% and the D retention to ± 50%.

The results show the D retention lies often below the detection limit or very close to it, only W shows significant retention at around 500 K. About 2×10^{20}/m² of C and O were found in the first resolution layer/surface on all samples, typical for all PSI-2 exposures. The values were not considered in the following discussion since they most probably relate to PSI-2 plasma impurities or the later air contact. Significantly higher sputtering yields were observed for the steels in the exposure at ~1100 K compared to ~520 K. The W surface enrichment on the steels was higher for lower temperatures, e.g. 7.5% vs. 5.8%. Interestingly the final enrichment follows roughly the initial W content in the bulk material. The mass-loss indicates a sputtering of 0.8 to 0.9 µm of steel. On the W reference samples, about 0.03 µm of material were lost due to impurity sputtering in PSI-2. The W enrichment on the steels originates from preferential sputtering of the Fe and Cr constituents. Compositional depth profiles by RBS show an enrichment of W and Cr towards the plasma-loaded surface, see the example in Fig. 4. The separation of Fe and Cr has a significant error bar due to the partial signal overlap, but the data are conclusive in the shown range. For ~520 K, the compositional differences from the bulk values restrict to the first resolution range of 20 nm (ResolNRA), but for 1150 K, differences were observed to about 1 µm depth.

The surface analysis by electron microscopy and focussed-ion-beam cutting revealed distinct differences between the high and low temperature exposures. Fig. 5 displays the surface of HiperFer W6 after exposure to 526 K and Fig. 6 after exposure to 1069 K. A grass-like surface with 50 nm peak to valley has developed at 526 K, while it was coarser at 1069 K with dimension in the 1 µm range. In both cases, the structure seemed homogeneously impregnated by W, according to energy-dispersive-x-ray (EDX) analysis at 3 keV electron energy. EDX shows about the same enrichment of W for the low-temperature exposures as RBS, but for the higher temperatures, the EDX values exceed the RBS values by about 50%. The differences arise from the depth averaging of EDX compared to the depth resolution of RBS. Within the surface, numerous particles of Mo-Nb are embedded, covering about 0.3% of the surface. From the electron microscopy results it remains unclear whether the reduced sputtering yield originates from the nano-structured surface, which could lead up to a factor 5 reduction in sputtering yield according to recent simulations [19], or the W enrichment, or even the combination of both effects.

For improving the understanding of sputtering, a dynamic SDTrim.SP5 simulation with 70 eV ion impact energy, 10^{-3} O/D^+ impurity level, and HiperFer W6 surface was conducted. The D concentration was limited to 0.1, the O concentration to 0.01 and the standard binding energies were selected. The simulation ran for 10^9 numerical particles to achieve the experimental flux of 8.6×10^{25} D/m² with acceptable numerical accuracy. Diffusion was not considered. Therefore, the simulations mimic mostly the 520 K exposure where also no metal diffusion became apparent in the RBS data. The simulations yield a strong drop of the Fe sputtering yield from initially 2.7×10^{-3} to 3.3×10^{-4} within 1.6×10^{25} D/m². The Fe concentration and effective yield stays constant afterwards, and it seems to be limited by the bulk Fe/W mixture ratio and the W sputtering yield of 4.7×10^{-6}. In summary, the simulation suggests the ratio of Fe/W inverts in the plasma affected depth (1.2% Fe in surface vs. 1.2% W in bulk). The modelled yield averaged over the experimental fluence reads 5×10^{-4} (Fe + Cr)/D, in rough agreement with the experimental value of $7.9 \pm 2 \times 10^{-4}$ /D considering the systematic uncertainty of the ion impact energy and impurity level in PSI-2. The enrichment limits to a thin surface near layer of 2 ± 1 nm (ion penetration depth). These values roughly agree with the RBS data when averaging over 20 nm instead, supposing the W enrichment plays the major role in sputter yield reduction.

The surface power loading capability was analysed carrying out a 2D finite element analysis (FEA). In a transient structural environment, a mockup design of a plasma-facing component (PFC) was modelled using direct-coupled thermal-structural elements. The left part of Fig. 7 depicts the geometry along with relevant boundary conditions. A multilinear isotropic hardening model, elastic-plastic mechanical behaviour, and a heat transfer coefficient of 128 W/(m²K) between metal and cooling water were assumed.

The selection of material properties was based on the assumption that HiperFer behaves similar to Crofer22H [20] for the given temperature range, for the values not available for HiperFer. As for the geometry of the PFC, the coolant tube was extended with a 3 mm thick HiperFer armour towards the plasma, following design suggestions for W armour PFCs by Igitkhanov et al. [21,22] and Heuer et al. [23]. At a coolant temperature of 473 K, a power load of 3 MW/m² to the top surface results in 1113 K maximum surface temperature, Fig. 7(a) and Table 3.

At 1 MW/m² the surface temperature maximum reduces to 708 K and a difference of 235 K to the coolant temperature, respectively. With the mockup design, von Mises stresses of ~252 MPa occur at the edges of the water tube, Fig. 7(b), for all heat loads above 1 MW/m². In W armoured PFCs of a similar design as applied here, detrimental σ_{yy} stresses of 1050 MPa and plastic deformations are reported to exist at the transition of the steel structure to the W armour due to a dissimilar materials joint [23], both of which could be avoided with a Hiperfer monoblock design. In currently envisaged PFCs for DEMO, these loads will be crucial, too. Using a single-material (HiperFer) PFC design

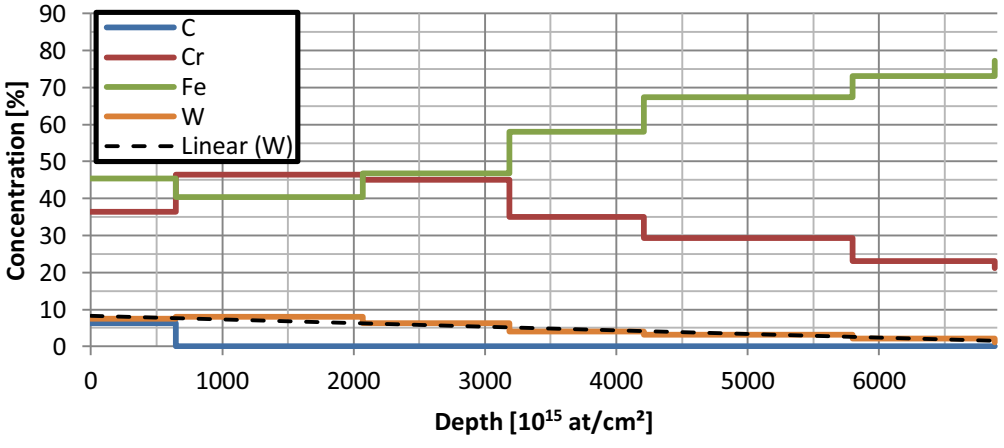

Fig. 4. Compositional depth profile down to ~825 nm of the HiperFer W6 sample exposed at 1069 K measured by RBS (Fe, W, Cr) and NRA (C). The results indicate an enrichment of Cr, W, Nb, and Mo (plasma impurity) at the surface, while Fe gets depleted. The W enrichment follows a linear decay in depth (dotted line). After the depicted range, the composition recovers the bulk quantities.

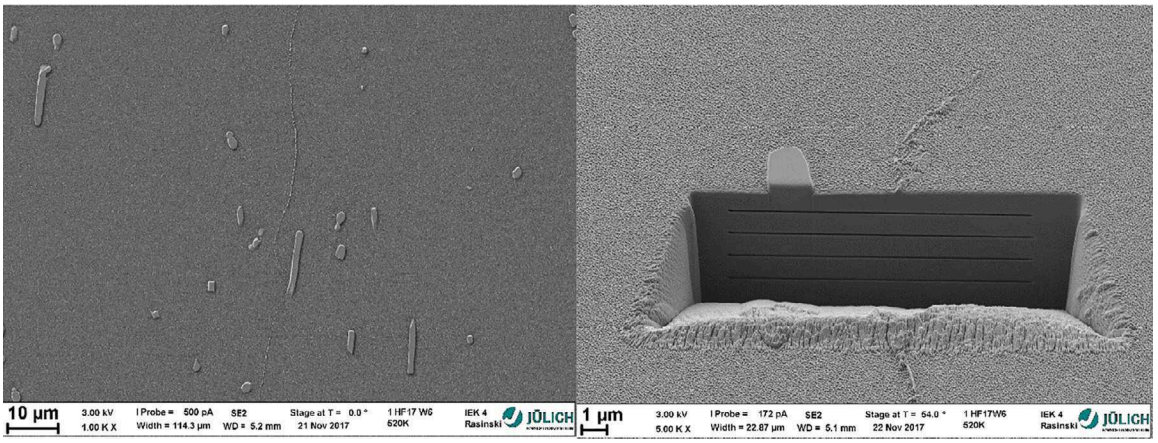

Fig. 5. Electron microscopy images of HiperFer-W6 after PSI-2 exposure at 526 K. The left picture shows the surface with a central grain boundary and several Mo–Nb islands. In total, the islands cover about 0.3% of the surface area. Mo originates from the PSI-2 plasma source. The right image shows a FIB-cut at one of these islands. The island has a height of about 300 nm. Furthermore, the surface formed a grass like structure, probably responsible for the reduced sputtering yield. EDX analysis revealed a homogeneous distribution of W over the surface, including the islands.

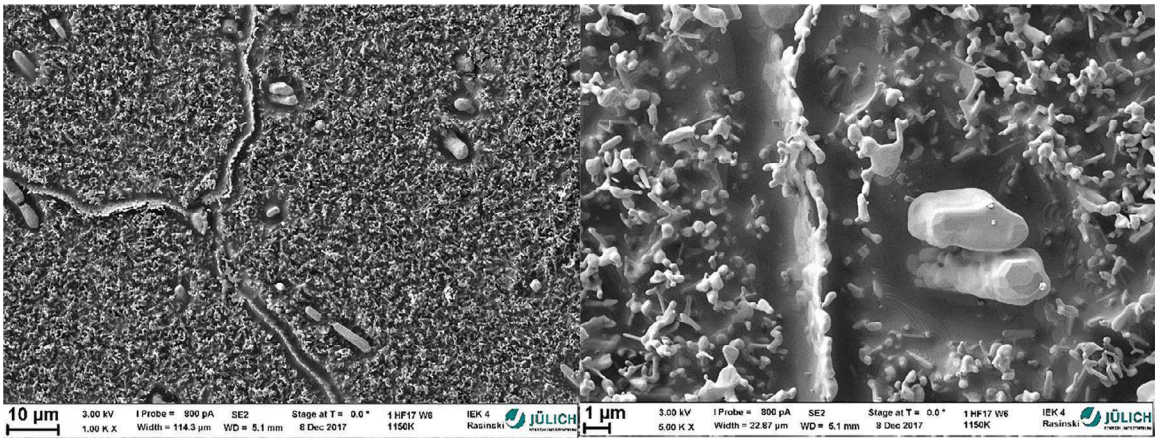

Fig. 6. SEM image of HiperFer-W6 after exposure at 1069 K. As in Fig. 5, Mo–Nb crystallites are visible throughout the surface. W enriched at the grain boundary lines and the fuzzy structures. The fuzzy structures grow coarser at higher temperatures.

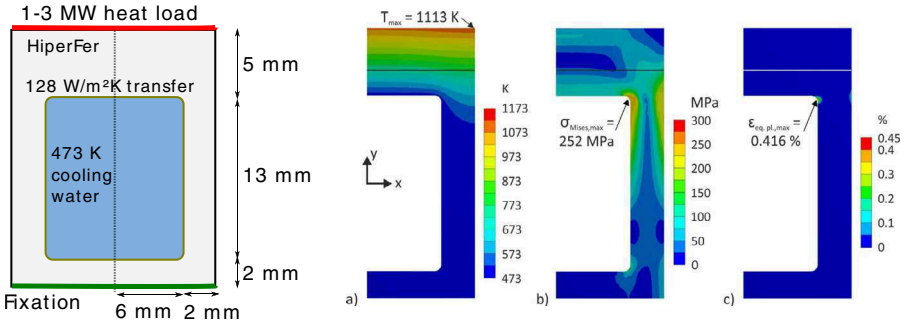

Fig. 7. Left: Geometry of the FEA along with relevant boundary and symmetry conditions, similar to analyses by Rayaprolu et al. [15], Möller et al. [16] and Mayer [17] for W armour PFCs. Right: Results of the FEA considering a heat load of 3 MW/m^2 to the top surface of the geometry. Only the right half of the bilaterally symmetric component is shown for each result. (a) temperature distribution, (b) von Mises stress distribution, (c) equivalent plastic strain distribution. The location of each maximum remains for lower heat loads.

would ease the thermo-mechanical stress profile significantly. While the optimal design has yet to be evaluated, HiperFer can already handle loads of approximately 1.5 MW/m^2 with the suggested mockup.

5. Conclusions

We demonstrated the proof-of-principle for a new steel, called HiperFer, feasible for plasma-facing and structural components in a nuclear fusion reactor. The material, developed for high-temperature steam power plants, already demonstrated its excellent high temperature mechanical and fatigue properties in the literature. The new material follows the main ideas of Eu-97, but in contrast features only the ferritic phase, higher Cr content for steam oxidation resistance, a higher W content, and a different strengthening mechanism leading potentially to benefits under fusion conditions.

The activation modelling analysis demonstrated low activity levels of the order of pure Fe in particular due to low contents of C and N impurities of the ferritic phase. The modelling revealed the possibility of non-active release after use in fusion reactors after 1000 years of cooling time with large uncertainties requiring experimental validation,

Table 3
Effect of heat loads to the top edge of the selected FEA geometry on the maximum temperature, maximum von Mises stress and maximum plastic strain with 473 K coolant temperature. Locations of each results are indicated by Fig. 7.

Heat load (MW/m^2)	T_{Max} (K)	Max. von Mises stresses (MPa)	Max. plastic deformation (%)
1	708	191	0
1.5	815	257	0.023
2	914	249	0.124
2.5	1013	249	0.261
3	1113	252	0.416

especially due to uncertainties in the nuclear cross-sections. Robust conclusions can only be drawn knowing the final material production and irradiation conditions.

In PSI-2, different grades of HiperFer and W were investigated for sputtering and deuterium retention. Exposure at ion impact energies between the Fe and the W threshold lead to a 30 times higher sputtering yield of HiperFer compared to pure W, but simulations indicate only the first 25% of the exposure time lead to significant sputtering while the build-up of an enriched W layer protected the material in the remaining 75% of the exposure. The total sputtering yields of HiperFer compare well to SD.Trim.SP simulations in the 520 K exposure, but temperatures of about 1150 K during plasma exposure suppressed the evolution of a sputter resistant surface within the applied plasma flux and exposure time. The apparent W enrichment at 520 K reached levels of about 8% within the depth resolution of 20 nm, leading to a reduction of the total sputtering yield of a factor 4.3 compared to exposures at 1150 K or pure Fe. Alterations of the steels material properties due to depletion of iron by preferential sputtering cannot be expected, since even at 1150 K only the first 1 μm was depleted of iron within the 4 h exposures. Ion-beam analysis revealed ppm levels of deuterium retention in HiperFer, mostly independent of exposure parameters. Along with thermo-mechanical modelling of a plasma-facing component, the application of HiperFer in plasma-facing components with loads in the order of 1.5 MW/m^2 is feasible. Designs optimized for HiperFer offer prospects of further increasing this value.

HiperFer's unique high-temperature strength due to Laves-phase hardening potentially solves several vicious circles, e.g. regarding α-α' unmixing and its contradiction to excellent self-passivation or mechanical strength vs. defect annealing and outgassing with respect to temperature. The unification of functional and structural materials, manageable nuclear waste and high coolant temperatures for efficient energy conversion offered by HiperFer open prospects for significant cost reductions in fusion reactor design, manufacturing, and maintenance, boosting the economical acceptance of nuclear fusion. Furthermore, also the social acceptance of nuclear fusion would profit from reduced nuclear waste and improved passive safety. This and the promising results presented here justify further efforts towards more experimental studies of HiperFer. In the next steps, the production of an optimized HiperFer-Ta batch for manufacturing of plasma-facing components and irradiation tests in accelerators are envisaged.

Acknowledgement

This project has received funding from the European Union's Horizon 2020 research and innovation programme under grant agreement number 633053. The views and opinions expressed herein do not necessarily reflect those of the European Commission.

References

[1] M. Rieth, et al., FZKA 6911, Eurofer 97, Forschungszentrum Karlsruhe (2003).
[2] D. Stork, et al., Assessment of the EU R&D programme on DEMO structural and high-heat flux materials, EFDA, 2012.
[3] B. Kuhn, M. Talik, L. Niewolak, J. Zurek, H. Hattendorf, P. Ennis, W.J. Quadakkers, T. Beck, L. Singheiser, Development of high chromium ferritic steels strengthened by intermetallic phases, Mater. Sci. Eng. A594 (2014) 372–380.
[4] A. Kreter, C. Brandt, A. Huber, S. Kraus, S. Möller, M. Reinhart, B. Schweer, G. Sergienko, B. Unterberg, Linear plasma device PSI-2 for plasma-material interaction studies, Fusion Sci. Technol. 68 (2015) 8–14, https://doi.org/10.13182/FST14-906.
[5] B. Kuhn, M. Talik, T. Fischer, Y. Yamamoto, J.L. Barrilao, X. Fan, Mechanical properties and application potentials of high performance ferritic (HiperFer) steels, 4th International ECCC Creep & Fracture Conference, 2017.
[6] R. Lindau, et al., Present development status of EUROFER and ODS-EUROFER for application in blanket concepts, Fusion Eng. Des. 75-79 (2005) 989–996.
[7] European Creep Collaborative Committee, ECCC-Datasheets, 2014.
[8] T. Goorley, et al., Initial MCNP6 release overview, Nucl. Technol. 180 (2012) 298–315.
[9] S. J.C., E. J.W., M. J.G., F. M., G. M.R., The FISPACT-II User Manual, (2016) CCFE-R (11) 11 Issue 8 http://fispact.ukaea.uk.
[10] M. Gilbert, C. Bachmann, U. Fischer, N. Taylor, Activation, decay heat, and waste classification studies of the European DEMO concept, Nucl. Fusion 57 (2017), https://doi.org/10.1088/1741-4326/aa5bd7.
[11] A.J. Koning, et al., TENDL-2015, https://tendl.web.psi.ch/tendl_2015/alpha_html/Ge/AlphaGe.html, (2016).
[12] M. Gilbert, J.C. Sublet, CCFE-R(16)36, http://www.ccfe.ac.uk/fispact_handbooks.aspx, (2016).
[13] J. Harmann, DEMO operational concept description. 2012. EFDA Report no. 2LCY7A.
[14] M. Mathon, Y. d. Carlan, G. Geoffroy, X. Averty, A. Alamo, C.H. d. Novion, A SANS investigation of the irradiation-enhanced a–a' phases separation in 7–12 Cr martensitic steels, J. Nucl. Mater. 312 (2003) 236–248.
[15] R. Rayaprolu, S. Möller, C. Linsmeier, S. Spellerberg, Simulation of neutron irradiation damage in tungsten using higher energy protons, Nucl. Mater. Energy 9 (2016) 29–35, https://doi.org/10.1016/j.nme.2016.09.008.
[16] S. Möller, O. Kachko, M. Rasinski, A. Kreter, C. Linsmeier, In situ investigation of helium fuzz growth on tungsten in relation to ion flux, fluence, surface temperature and ion energy using infrared imaging in PSI-2, Phys. Scr. T170 (2017) 014017(6pp).
[17] M. Mayer, SimNRA User´s Guide, Max-Planck-Institut für Plasmaphysik, Garching, 1997 IPP Report Number: IPP 9/113 www.simnra.com.
[18] T. Silva, C. Rodrigues, M. Mayer, M. Moro, G. Trindade, F. Aguirre, N. Added, M. Rizzutto, M. Tabacniks, MultiSIMNRA: a computational tool for self-consistent ion beam analysis using SIMNRA, Nucl. Instrum. Methods 371 (2016) 86–89.
[19] U. v. Toussaint, A. Mutzke, A. Manhard, Sputtering of rough surfaces: a 3D simulation study, Phys. Scr. T170 (2017), https://doi.org/10.1088/1402-4896/aa90be.
[20] Thyssenkrupp VDM GmbH, VDM Crofer 22 H Material Data Sheet No. 4050, (2010) VDM Metals.
[21] Y. Igitkhanov, B. Bazylev, R. Fetzer, The Quantification of the Key Physics Parameters for the DEMO Fusion Power Reactor and Analysis of the Reactor Relevant Physics Issues (2014).
[22] Y. Igitkhanov, R. Fetzer, B. Bazylev, Effect of design geometry of the demo first wall on the plasma heat load, Nucl. Mater. Energy 9 (2016) 560–564.
[23] S. Heuer, T. Weber, G. Pintsuk, J.W. Coenen, J. Matejicek, C. Linsmeier, Aiming at understanding thermo-mechanical loads in the first wall of DEMO: Stress–strain evolution in a Eurofer-tungsten test component featuring a functionally graded interlay, Fusion Engineering and Design 135 (2018) 141–153.